Pattern-induced thermal unbinding of filaments

O. Pierre-Louis
LPMCN, Université Lyon 1, 43 Boulevard du 11 Novembre, F-69622 Villeurbane, France
(Received 21 June 2010; revised manuscript received 21 October 2010; published 11 January 2011)

Substrate patterning is shown to be a convenient method to control the adhesion of filaments. The pattern not only permits a control of adhesion, it also leads to an unbinding transition at finite temperatures. The dimensionality of transverse fluctuations controls the continuity of the transition, and in some cases, re-entrant binding is observed as temperature is increased. Unbinding on patterns is found to be easier to observe than unbinding on flat substrates. Finally, experimental conditions under which unbinding could be observable are discussed.

DOI: 10.1103/PhysRevE.83.011801 PACS number(s): 36.20.−r, 87.16.Ka, 05.20.Gg

I. INTRODUCTION

Recent progress in surface topographical patterning now allows one to design patterns with periodicities around 100 nm. Novel techniques based on self-organization may allow one to reach even smaller length scales [1,2]. This mastering of surface patterning opens novel possibilities for controlling adhesion of various objects, such as liquid drops [3], solid clusters [4], membranes [5], and biological cells [6]. In the following, the consequences of surface patterning on filament adhesion are discussed.

In the past decades, the adhesion of polymers and filaments on flat substrates has given rise to a considerable literature. Among pioneering theoretical studies, the works of Rubin [7], de Gennes [8], and Wiegel [9] have pointed out the existence of an unbinding transition for flexible polymers on flat substrates at a temperature T_f. Below T_f the polymer sticks to the substrate, while above T_f it unbinds. Following these early works, several improvements of these models have been performed, such as better treatment of overhangs [10,11].

Recently, nanophysics and biophysics have brought attention to the so-called semiflexible filaments, such as carbon nanotubes or actin filaments, which exhibit a large bending rigidity. Semiflexible filaments also exhibit an unbinding transition on flat substrates, which may be continuous or discontinuous depending on the dimensionality of transverse fluctuations [12–14].

Although there has been some work considering the role of the corrugation of the potential in the literature [15,16], there is, to our knowledge, no study showing an unbinding transition induced by the pattern. In the following, it is shown that filament adhesion can be controlled by surface patterning. A suitable choice of patterns may not only tune the adhesion strength, it may also completely forbid adhesion by inducing an unbinding transition which differs qualitatively from the transition on flat substrates.

First, we shall recall the nontrivial zero-temperature limit experienced by filaments on patterns [17]. A formulation will then be established in the presence of a nonzero temperature. The resulting model will be solved for a sinusoidal substrate profile with a combination of numerical and analytical tools. A single transition line is shown to emerge at finite temperatures, which accounts for a pattern-induced unbinding transition. Finally, the relevance of this transition for actin adhesion on parallel grooves, and for DNA adhesion along atomic steps [18,19] will be discussed.

II. ZERO-TEMPERATURE LIMIT

Before including the consequences of thermal fluctuations, let us consider the zero-temperature limit, where the filament configurations would be those which minimize the energy $\mathcal{E}_0$ of the filament. For a filament along the x axis, with transverse displacements $h(x)$ and a substrate of height $h_s(x)$, one has in the small slope limit

$$\mathcal{E}_0 = \int dx \frac{C}{2}[\partial_{xx}h(x)]^2 - \int dx\, \gamma_0 \Theta_s[h(x)], \qquad (1)$$

where C is the bending modulus and γ_0 is the adhesion energy per unit length. The interaction between the filament and the substrate is a δ-function attraction at the surface of the substrate, plus the repulsive hard core of the substrate. Integrating this energy over the possible transverse displacements, we obtain the second term of Eq. (1). The function $\Theta_s[h(x)]$ vanishes for $h(x) > h_s(x)$, is equal to 1 when $h(x) = h_s(x)$, and diverges for $h(x) < h_s(x)$ to forbid the penetration of the filament inside the solid.

The minimization of $\mathcal{E}_0$ on periodic substrate patterns with sinusoidal and fakir carpet profiles was reported in Ref. [17]. The ground state, i.e., the state of lowest energy, depends on a single parameter,

$$\alpha = (\kappa_{\rm eq}/\kappa_g)^{1/2}, \qquad (2)$$

where $\kappa_{\rm eq} = (2\gamma_0/C)^{1/2}$ is the equilibrium local curvature at contact points where the filament reaches the substrate, and $\kappa_g = 4\pi^2\epsilon/\lambda^2$ is the typical substrate curvature for a pattern with wavelength λ, and amplitude $\epsilon \ll \lambda$. When α is large, e.g., for flat substrates, the ground state is full adhesion. Upon a decrease in α, the bending energy cost for the filament to adapt to patterns in the full adhesion state increases. When this cost becomes comparable with the adhesion energy gain, i.e., when $\alpha \sim 1$, it is more favorable for the filament to detach from the undulated substrate. A detailed analysis [17] reveals that, decreasing α, the ground state changes from the full adhesion state to a periodic state with detachment zones passing over one, then two, three, etc., pattern periods. Finally, the period of the ground state diverges when $\alpha \to \alpha_\infty$. The ground state is the unbound state for $\alpha < \alpha_\infty$. Hence there is an infinite series of ground-state transitions at zero temperature ended with an unbinding point.

It is usually expected that in one-dimensional systems with local interactions, zero-temperature transitions do not survive at finite temperature [20]. A well known example is that of the

Frenkel-Kontorova model, which exhibits an infinite series of zero-temperature ground-state transitions (forming a devil's staircase) becoming crossovers at any finite temperature [21]. In the case of filaments on patterned surfaces, this statement holds for the transitions from one periodic state to the other in the series of zero-temperature transitions. But it does not hold for the final zero-temperature unbinding transition at α_∞, which involves diverging length scales. In the following, these issues are addressed within a low-temperature approach.

III. LOW-TEMPERATURE FORMULATION

Let us start with the low-temperature formulation. The free parts are defined as parts of the filament not in contact with the substrate. The ends of these parts are in contact with the substrate at x_1 and x_2, where the bending energy enforces tangential matching [17]. Following Benetatos and Frey [14], the partition function of a free part at $x_1 < x < x_2$ reads $Z[x_1,x_2] = P[x_1,x_2]Z_{\rm fe}[x_2 - x_1]$, where $Z_{\rm fe}[x_2 - x_1]$ is the partition function of a filament of length $x_2 - x_1$ with free ends. The precise expression of $Z_{\rm fe}$ depends on the specific properties of the filament, and is actually irrelevant in the following. In the limit where $x_2 - x_1$ is smaller than the persistence length $L_p = 2C/k_BT$, the Green's function formalism of Ref. [14] provides

$$P[x_1,x_2] = \left(\frac{3^{1/2}CB}{\pi k_BT}\right)^d \frac{e^{-(C/2k_BT)\int_{x_1}^{x_2} dx[\partial_{xx}\bar{h}(x)]^2}}{(x_2-x_1)^{2d}}, \qquad (3)$$

where d is the dimension of transverse fluctuations: $d = 1$ when fluctuations along z are allowed, and $d = 2$ when the filament can also fluctuate in the third direction y (see Fig. 1). The length scale $B = 4\delta h\delta\theta$ is built from a combination of allowance for microscopic transverse displacements δh and rotation angles $\delta\theta$ at the contact point. Note that instead of $h(x)$, the average filament position $\bar{h}(x)$, which obeys $\partial_{xxxx}\bar{h}(x) = 0$, enters in Eq. (3).

Furthermore, the partition function of a part of the filament in adhesion running from x_1 to x_2 may be written as $Z_a[x_1,x_2] = P_a[x_1,x_2]Z_{\rm fe}[x_2 - x_1]$, where

$$P_a[x_1,x_2] = e^{-\{(C/2)\int_{x_1}^{x_2} dx[\partial_{xx}h_s(x)]^2 - \gamma_T(x_2-x_1)\}/k_BT}, \qquad (4)$$

where γ_T is the adhesion free energy per unit length on a flat substrate at temperature T, so that $\gamma_T \to \gamma_0$ as $T \to 0$. The adhesion energy γ_T vanishes at a finite temperature T_f [12–14]. Here, temperatures well below this transition are considered, so that $\gamma_T > 0$, and the length of thermal bubbles (detachment zones induced by thermal fluctuations on flat substrates) are typically smaller than the pattern wavelength λ.

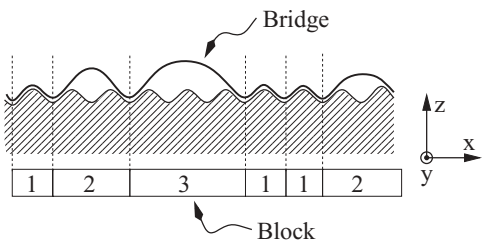

FIG. 1. Model schematics. A filament in adhesion on a periodically patterned substrate exhibits local metastable features, denoted as bridges, where the filament is not in adhesion. The global filament configuration is mapped to a lattice model with blocks of arbitrary length.

Combining Eqs. (3) and (4), one obtains the probability of a given configuration with m free parts starting at x_i^+ and ending at x_i^- with $x_i^+ < x_i^- < x_{i+1}^+$ as

$$\mathcal{P} = \prod_{i=1}^{m} P[x_i^-,x_i^+]P_a[x_i^+,x_{i+1}^-]. \qquad (5)$$

Upon the variation of the positions $x_i^\pm$, the probability $\mathcal{P}$ exhibits local maxima for some special values of $x_i^\pm$. These local maxima of $\mathcal{P}$ are local minima of the free energy, and correspond to metastable states.

Let us now specialize the discussion to the case of a sinusoidal pattern,

$$h_s(x) = -\epsilon\cos[2\pi x/\lambda], \qquad (6)$$

for which $\alpha_\infty \approx 0.791$ [17]. The metastable states are then composed of "bridges" of arbitrary length, as shown in Fig. 1. Bridges exhibit the $x \to -x$ symmetry. Using normal mode variables for dilatation

$$\xi = [n - (x^+ - x^-)/\lambda]/2 \qquad (7)$$

and translation

$$\delta = [n - (x^+ + x^-)/\lambda]/2, \qquad (8)$$

the maxima of $\mathcal{P}$ obey $\delta = \delta_n^* = 0$ and $\xi = \xi_n^*$, where

$$\alpha^2\left(1 + \frac{\zeta d}{(n-2\xi_n^*)}\right) = -\cos 2\pi\xi_n^* - \frac{\sin 2\pi\xi_n^*}{\pi(n-2\xi_n^*)}. \qquad (9)$$

These metastable states are the only ones which exist in the transition region, where $\alpha < 1$. The opposite regime $\alpha > 1$ is trivial because there is essentially no metastable state and the filament is always in full adhesion.

Within a low-temperature approach, the main contributions to the partition function will result from configurations which are in the vicinity of the local maxima of $\mathcal{P}$. Performing a saddle point expansion, the probability of a block of length $n\lambda$ with $n \geqslant 2$, consisting of a bridge and of the adhesion parts up to the nearest minima of the surface pattern (see Fig. 1), reads

$$P_n \approx \frac{2r}{(n-2\xi_n^*)^{2d}} \frac{2\pi\zeta e^{-e_n[\xi_n^*,0]/\zeta}}{(\partial_{\xi\xi}e_n[\xi_n^*,0]\partial_{\delta\delta}e_n[\xi_n^*,0])^{1/2}}, \qquad (10)$$

with the dimensionless parameters

$$\begin{aligned} \zeta &= k_BT/\lambda\gamma, \\ r &= (3^{1/2}CB/\pi k_BT)^d\lambda^{2d-2}L_m^{-2}. \end{aligned} \qquad (11)$$

We have also defined L_m as the microscopic distance between two possible positions of the contact points along x. Since $B \to 0$, one expects $r \ll 1$ [14]. Finally, the energy reads

$$\begin{aligned} e_n[\xi,\delta] = \xi\left(\frac{1}{\alpha^4} - 2\right) + \frac{c_{2\delta}s_{2\xi}}{4\pi\alpha^4} + \frac{c_\delta^2 s_\xi^2}{\pi^2\alpha^4(n-2\xi)} \\ + \frac{3s_\delta^2[\pi(n-2\xi)c_\xi + s_\xi]^2}{\pi^4\alpha^4(n-2\xi)^3}, \end{aligned} \qquad (12)$$

where $c_x = \cos 2\pi x$ and $s_x = \sin 2\pi x$. As shown in Fig. 1, one may also define a block of length λ consisting of a

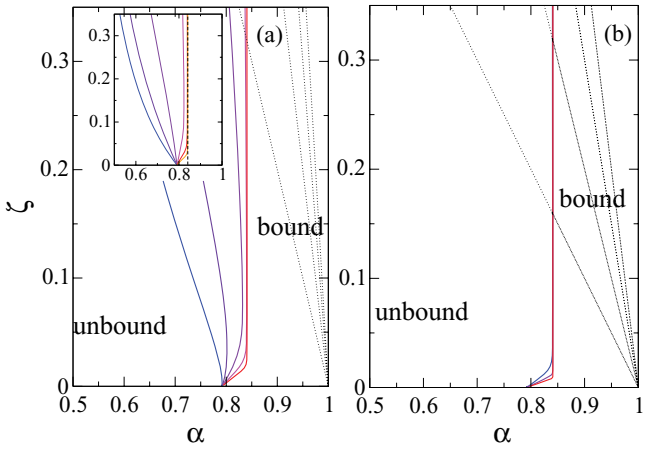

FIG. 2. (Color online) Phase diagram in the (α,ζ) plane. Solid lines represent the transition lines. From left to right, these lines correspond to increasing values of r (or R). Dotted lines represent the limit of existence of bridges, Eq. (13). (a) $d = 1$ with $r = 10^{-n}$, $n = 1,\ldots 5$. Inset: same plot at fixed $R = \zeta r\alpha^4$ for $R = 10^{-n}$, $n = 1,\ldots 6$. (b) $d = 2$, and $r = 10^{-1}, 10^{-3}, 10^{-5}$.

filament in full adhesion. The probability of this block is $P_1 = e^{-[1/(2\alpha^4)-1]/\zeta}$.

As shown in the following, the decomposition of the system into blocks allows one to calculate the partition function of the filament using well known methods which have been developed for the helix-coil transition, or the filament adhesion on flat substrates [12–14]. Nevertheless, one must keep in mind a major difference: Here detachment zones are metastable states, and not thermal bubbles such as those of the above mentioned models. This is the reason why filaments on patterns exhibit a nontrivial zero-temperature limit, whereas filaments on flat substrates are always bound at $T \to 0$. Another difference comes from restrictions on the domain of existence of a given bridge which arise from the request that the filament should not penetrate the solid. This restriction imposes

$$\alpha + \zeta d/2(n-1) < 1. \tag{13}$$

These conditions are represented by the dotted lines in the (α,ζ) plane in Fig. 2. One should set $P_n = 0$ when they are not satisfied.

IV. TRANSITION LINE

We shall now analyze the consequences of the model. The reduced partition function Z_N of a filament of length $N\lambda$ is defined as the total partition function divided by $Z_{\rm fe}[N\lambda]$. For definiteness, the filament is maintained at the surface at both ends. Considering all possible lengths $n = 1,\ldots,N$ for the first block in a system of size N, one obtains the recursion relation

$$Z_N = \sum_{n=1}^{N} P_n Z_{N-n}, \tag{14}$$

where $Z_0 = 1$. Using standard analysis (see Appendix A), this relation leads to

$$Z_N = \frac{1}{2i\pi}\oint d\phi\, \phi^{-N-1}\frac{A_\phi}{1-A_\phi}, \tag{15}$$

where the complex variable ϕ is analogous to a fugacity, and

$$A_\phi = \sum_{n=1}^{\infty} P_n \phi^n. \tag{16}$$

The integration contour in Eq. (15) encircles the origin [9]. In the ϕ plane, the argument of the integral in Eq. (15) exhibits a branch cut on the real axis for $\phi > 1$ and a simple (real positive) pole ϕ_0, solution of $A_{\phi_0} = 1$. Note that following Ref. [14], the suitable thermodynamic limit consists of keeping the filament length constant and smaller than $L_p = 2C/k_BT$, while $N \to \infty$ (i.e., $\lambda \to 0$). When $N \to \infty$, the partition function Z_N is dominated by the singularity which is the closest to the origin. When $\phi_0 < 1$, one has $Z_N \sim \phi_0^{-N}$, and the fraction χ of the filament which is in adhesion is finite. As $\phi_0 \to 1$, a transition occurs where $\chi \to 0$.

The numerical solution of the transition equation $\phi_0 = 1$, presented in Fig. 2, shows that a transition line emerges at finite temperatures. The transition occurs at finite α, corresponding to $\gamma_T > 0$, and thus to $T < T_f$. This proves the self-consistency of the model, which assumes *a priori* $T < T_f$.

As $r \to 0$, the transition line tends to a well defined limit composed of a segment of the $\zeta = 0$ axis for $\alpha_\infty < \alpha < \tilde{\alpha} = 2^{-1/4}$, and of the line $\alpha = \tilde{\alpha}$. For nonvanishing r, two main changes appear. First, at small ζ, the transition occurs at α_c, with $\alpha_c - \alpha_\infty \sim -\zeta \ln r\zeta$. Second, at large ζ, the transition line deviates toward smaller α, with $\alpha_c \sim \zeta^{-1/3}r^{-1/6}$. This feature is observed only for $d = 1$ with $r > 10^{-4}$. For $d = 2$, it appears for unreasonably large values of r or ζ. Since $r \sim 1/T$ depends on T, the consequences of a variation of T is difficult to infer from the plots at fixed r in Fig. 2(a). However, the inset of Fig. 2(a) shows the transition lines for fixed values of the temperature-independent parameter,

$$R = r\zeta\alpha^4 = 3^{1/2}B\lambda^3/\left(8\pi^4 L_m^2\epsilon^2\right). \tag{17}$$

One still finds a decrease of α as ζ is increased when $d = 1$ and $R > 10^{-4}$. As $T \to 0$, one has $\gamma_T \to \gamma_0$, so that an increase of T corresponds to a vertical trajectory from the $\zeta = 0$ axis at fixed R. One may therefore conclude from the inset of Fig. 2(a) that binding can be obtained by increasing temperature for filaments that are unbound at zero temperature when $\alpha < \alpha_\infty$, $d = 1$, and $R > 10^{-4}$.

In addition, the transition lines exhibit kinks when they cross the lines given by the inequalities (13). However, these kinks are too small to be seen in Fig. 2, and probably cannot be observed in experiments.

V. ADHESION FRACTION

The fraction χ_N of filament in contact with the substrate can also be calculated numerically from the recursion relation (see Appendix B),

$$\chi_N = 1 - \sum_{n=1}^{N}\frac{Z_{n'}}{NZ_N}[N - 2\xi_n^* - n'\chi_{n'}]P_n, \tag{18}$$

where $n' = N - n$ and $\chi_0 = 0$. Figures 3(a) and 3(b) indicate that the transition is continuous for $d = 1$ and discontinuous for $d = 2$, as already noticed by several authors for the

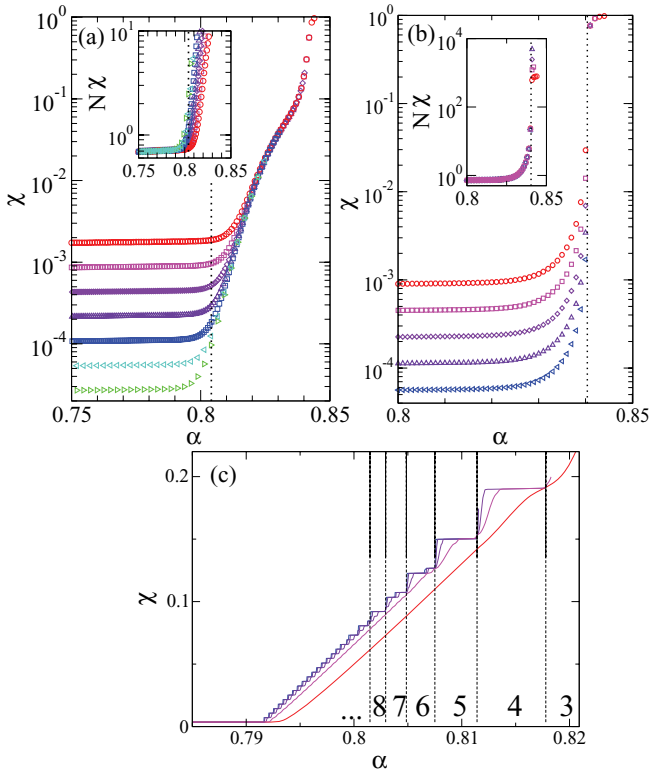

FIG. 3. (Color online) Fraction χ_N of filament in adhesion with the substrate obtained from a numerical evaluation of Eq. (18). The unbinding transitions are indicated by a dotted line. (a) Continuous transition for $d = 1$, $r = 10^{-4}$, $\zeta = 0.01$, and $N = 100 \times 2^n$, with $n = 2, \ldots, 8$. (b) Discontinuous transition for $d = 2$, $r = 0.1$, $\zeta = 0.02$, and $N = 100 \times 2^n$, with $n = 3, \ldots, 8$. The insets show data collapse for $N\chi$ with different values of N when $\alpha < \alpha_c$. (c) Low-temperature behavior for $r = 10^{-2}$, $N = 200$, and $d = 1$. The period n_G of the ground state at zero temperature is indicated at the bottom of the graph. The zero-temperature transitions from one periodic ground state to the other are blurred as the temperature increases, $\zeta = 10^{-5}, 3 \times 10^{-5}, 10^{-4}, 3 \times 10^{-4}, 10^{-3}$.

transition on flat substrates [13,14]. Since we artificially force the filament ends to be in contact with the substrate, χ_N does not vanish in the detached phase, but $\chi_N \sim N^{-1}$, as shown in the insets of Figs. 3(a) and 3(b). At zero temperature, the ground state consists of the repetition of a given block of size n_G when $\alpha > \alpha_\infty$ [17]. Each value of n_G corresponds to a well defined value of χ_N, leading to a series of steps at zero temperature in Fig. 3(c). As announced earlier, these transitions become smooth crossovers at any nonzero temperature. Note that additional small steps in χ_N appear at low temperatures as a consequence of finite size effects.

VI. EFFECTIVE ADHESION FREE ENERGY

Patterns do not only induce an unbinding transition, they are also a convenient way to control the adhesion energy of filaments. The strength of the adhesion between the filament and substrate is measured by the effective adhesion energy per unit length $\gamma_{\rm eff}$, which is defined as the difference between the full free energy minus the free energy of a filament in absence of contact with the substrate. We have

$$\gamma_{\rm eff} = \frac{k_B T}{N\lambda} \ln Z_N. \tag{19}$$

The value of $\gamma_{\rm eff}$, shown in Fig. 4, is obtained from a numerical integration of the recurrence relation (14) for a system of size $N = 200$. Above the transition, when $\chi \to 1$, the effective adhesion energy $\gamma_{\rm eff}$ tends to the adhesion energy in the full adhesion state,

$$\gamma_{\rm fa} = \gamma_T \left(1 - \frac{1}{2\alpha^4}\right). \tag{20}$$

Below the transition, $\gamma_{\rm eff} \to 0$. The small negative value of $\gamma_{\rm eff}$ observed in Fig. 4 below the transition is due to finite size effects, and vanishes as $N \to \infty$.

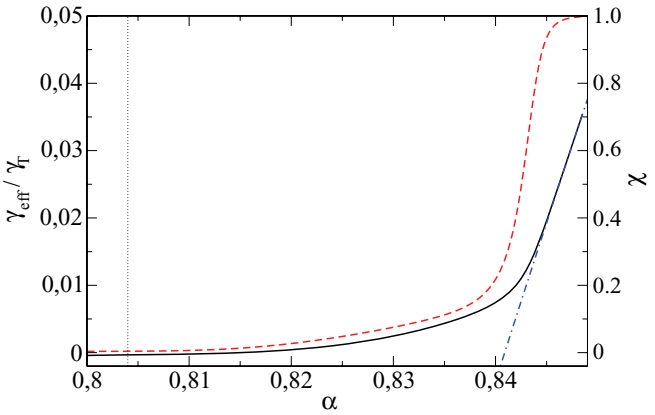

FIG. 4. (Color online) Effective adhesion energy. Model parameters: $N = 200$, $\zeta = 0.01$, $d = 1$, and $r = 10^{-3}$. Black solid line: effective adhesion energy $\gamma_{\rm eff}/\gamma_T$. Red dashed line: adhesion fraction χ. Blue dashed-dotted line: adhesion energy in the full adhesion state.

VII. DISCUSSION

A. Actin filament maintained perpendicularly to parallel grooves

Let us now turn to specific examples, and consider an actin filament with $C \sim 6 \times 10^{-26}$ J m [22], attached to a functionalized substrate with a line of binding molecules having a binding energy $J \sim k_B T$. The spacing between the binders is chosen to be 5 nm. Following Ref. [14], the transition on flat substrates should be observed for

$$(J/k_B T_f)^2 (e^{J/k_B T_f} - 1) \approx 2\left(L_m^2 J^2 / CB\right)^2, \tag{21}$$

leading to $T \approx 2000$ K, which is too large to be observable. However, unbinding can be observed at room temperature via a suitable variation of the pattern geometry. Indeed, let us consider a sinusoidal pattern, with parallel grooves perpendicular to the line of binders, and $\epsilon \sim 50$ nm. Upon the variation of λ, unbinding occurs for $\lambda \sim 700$ nm at room temperature.

B. DNA along atomic steps

Another system of interest is DNA along atomic steps, where a continuous transition is expected ($d = 1$). Although

experiments are available on vicinal Si(111) substrates [18] and on sapphire steps [19], no systematic experimental study has been reported, to our knowledge. Steps may exhibit thermal roughness or nonequilibrium periodic meandering patterns [2]. Using $\epsilon \sim 1$ nm, $\lambda \sim 10$ nm, with $L_p = 2C/k_BT \sim 50$ nm, one finds that the adhesion transition occurs for $\gamma \sim k_BT$ per nm, which is the typical adhesion energy expected along a step from van der Waals interactions.[1] However, strictly speaking, the length of the filament should not be much larger than L_p, and our results only apply to short DNA.

VIII. CONCLUSION

In conclusion, filaments on patterned surfaces exhibit a pattern-induced unbinding transition at finite temperature, which is distinct from the unbinding transition on flat substrates. The results are not specific to sinusoidal patterns, and other profiles, such as fakir carpet [17] and sawtooth [23], which exhibit similar series of transitions at zero temperature, should also experience an unbinding transition at finite temperature. In addition, this transition could be observable for actin filaments on parallel grooves, or for DNA along atomic steps.

ACKNOWLEDGMENTS

The author wishes to thank A. Andreanov, R. Stinchcombe, and J. Yeomans for useful discussions, and the kind hospitality of J. Yeomans in Oxford where part of this work was performed.

APPENDIX A: THE PARTITION FUNCTION Z_N

The recurrence equation

$$Z_N = \sum_{n=1}^{N} P_n Z_{N-n} \tag{A1}$$

was obtained in the main text. The generating function is defined as [9]

$$Z_\phi = \sum_{n=1}^{N} \phi^N Z_N. \tag{A2}$$

Combining Eqs. (A1) and (A2), one finds

$$\begin{aligned} Z_\phi &= \sum_{N=1}^{\infty} \phi^N \sum_{n=1}^{N} P_n Z_{N-n} \\ &= \sum_{N=1}^{\infty} \sum_{n=1}^{N} P_n \phi^n Z_{N-n} \phi^{N-n} \\ &= \sum_{m=0}^{\infty} \sum_{n=1}^{\infty} P_n \phi^n Z_m \phi^m \\ &= \sum_{n=1}^{\infty} P_n \phi^n (Z_\phi + 1), \end{aligned} \tag{A3}$$

where in the third line we have used the new summation variable $m = N - n$, with $0 \leqslant m \leqslant \infty$. We now have

$$Z_\phi = \frac{A_\phi}{1 - A_\phi}, \tag{A4}$$

where

$$A_\phi = \sum_{n=1}^{\infty} P_n \phi^n. \tag{A5}$$

Finally one obtains Eq. (15) of the main text,

$$Z_N = \frac{1}{N!} \partial_\phi^N Z_\phi|_{\phi=0} = \frac{1}{2i\pi} \oint \phi^{-N-1} Z_\phi, \tag{A6}$$

where the integration contour encircles the origin.

APPENDIX B: RECURRENCE RELATION FOR THE ADHESION FRACTION χ_N

The length of a bridge in a block divided by λ reads

$$x_n = n - 2\xi_n^*. \tag{B1}$$

The expectation value of the sum of the lengths of the bridges in a system of length $N\lambda$ is

$$\Xi_n = \frac{1}{Z_N} \sum_{\{n_i\} \in \mathcal{R}[N]} \left(\sum_i x_{n_i} \right) \Pi_i P_{n_i}, \tag{B2}$$

where $\mathcal{R}[N]$ denotes the ensemble of the ordered lists $\{n_i\}$ of integers which obey $\sum_i n_i = N$. Hence $\mathcal{R}[N]$ represents all the different ways to cover the system of size N with blocks of length n_i. A recursion equation is then obtained as follows:

$$\begin{aligned} \Xi_N Z_N &= \sum_{\{n_i\} \in \mathcal{R}[N]} \left(\sum_i x_{n_i} \right) \Pi_i P_{n_i} \\ &= P_1 \sum_{\{n_i\} \in \mathcal{R}[N-1]} \left(x_1 + \sum_i x_{n_i} \right) \Pi_i P_{n_i} \\ &\quad + P_2 \sum_{\{n_i\} \in \mathcal{R}[N-2]} \left(x_1 + \sum_i x_{n_i} \right) \Pi_i P_{n_i} + \cdots + P_N x_N \\ &= P_1 (x_1 Z_{N-1} + \Xi_{N-1} Z_{N-1}) \\ &\quad + P_2 (x_1 Z_{N-2} + \Xi_{N-2} Z_{N-2}) + \cdots \\ &\quad + P_N (x_N Z_0 + \Xi_0 Z_0) \\ &= \sum_{n=1}^{N} (x_n + \Xi_{N-n}) Z_{N-n}, \end{aligned} \tag{B3}$$

where we have defined $\Xi_0 = 0$. Finally, using Eq. (B1) and the relation

$$\Xi_N = N(1 - \chi_N), \tag{B4}$$

one obtains Eq. (18) of the main text.

[1] Choosing van der Waals potential $U = A/r^6$, where r is the distance between a small substrate volume and a small DNA volume, one finds $\gamma \sim (3\pi^2/32) A a_0 \ell_0 / r_0^4$, where r_0 is the DNA-step distance, a_0 is the step height, and ℓ_0 is the DNA section radius. Choosing $a_0 = 0.6$ nm [18], $\ell_0 = d_0 \approx 1.2$ nm, and $A \sim 10^{-20}$ J (in water), one finds $\gamma \sim k_BT$ per nm.

[1] S. O. Kim *et al.*, Nature (London) **424**, 411 (2003).
[2] C. Misbah, O. Pierre-Louis, and Y. Saito, Rev. Mod. Phys. **82**, 981 (2010).
[3] D. Quéré, Rep. Prog. Phys. **68**, 2495 (2005).
[4] O. Pierre-Louis and Y. Saito, Europhys. Lett. **86**, 46004 (2009).
[5] P. S. Swain and D. Andelman, Phys. Rev. E **63**, 051911 (2001).
[6] J. L. Tan, J. Tien, D. M. Pirone, D. S. Gray, K. Bhadriraju, and C. S. Chen, Proc. Natl. Acad. Sci. USA **100**, 1484 (2003).
[7] R. Rubin, J. Chem. Phys. **43**, 2392 (1965).
[8] P. de Gennes, Rep. Prog. Phys. **32**, 187 (1969).
[9] F. Wiegel, *Phase Transitions and Critical Phenomena* (Academic, London, 1983), Vol. 7.
[10] D. B. Abraham, Phys. Rev. Lett. **44**, 1165 (1980).
[11] D. B. Abraham and F. T. Latrémolière, Phys. Rev. Lett. **77**, 171 (1996).
[12] A. Maggs, D. Huse, and S. Leibler, Europhys. Lett. **8**, 615 (1989).
[13] R. Bundschuh and M. Lässig, Phys. Rev. E **65**, 061502 (2002).
[14] P. Benetatos and E. Frey, Phys. Rev. E **67**, 051108 (2003).
[15] M. B. Hochrein, J. A. Leierseder, L. Golubovi, and J. O. Rädler, Phys. Rev. E **75**, 021901 (2007).
[16] T. Burkhardt, J. Math. Phys. A **31**, L549 (1998).
[17] O. Pierre-Louis, Phys. Rev. E **78**, 021603 (2008).
[18] T. Arai, M. Tomitori, M. Saito, and E. Tamiya, Appl. Surf. Sci. **188**, 474 (2002).
[19] K. Yoshida, M. Yoshimoto, K. Sasaki, T. Ohnishi, T. Ushiki, J. Hitomi, S. Yamamoto, and M. Sigeno, Biophys. J. **74**, 1654 (1998).
[20] L. Landau and E. Lifshitz, *Statistical Physics* (Elsevier, New York, 1986), Vol. 5.
[21] W. Selke, *Phase Transitions and Critical Phenomena* (Academic, London, 1992), Vol. 15.
[22] Y. Arai *et al.*, Nature (London) **399**, 446 (1999).
[23] O. Pierre-Louis (unpublished).